Non-Linear Optical Activity of Chiral Bipyrimidine-Based Thin Films

Prescillia Nicolas, Stephania Abdallah, Ahmet Dok, Yovan de Coene, Olivier Jeannin, Nathalie Bellec, Jean-Pierre Malval, Thierry Verbiest, Koen Clays, Stijn Van Cleuvenbergen, et al.

ACES Asian Chemical Editorial Society

doi.org/10.1002/asia.202400112

CHEMISTRY AN ASIAN JOURNAL Research Article

www.chemasianj.org

Non-Linear Optical Activity of Chiral Bipyrimidine-Based Thin Films

Prescillia Nicolas,[a] Stephania Abdallah,[b] Ahmet Dok,[c] Yovan de Coene,[c] Olivier Jeannin,[a] Nathalie Bellec,[a] Jean-Pierre Malval,[b] Thierry Verbiest,[c] Koen Clays,[c] Stijn Van Cleuvenbergen,[c] Belkiz Bilgin-Eran,[d] Huriye Akdas-Kiliç,*[a, d] and Franck Camerel*[a]

An original series of bipyrimidine-based chromophores featuring alkoxystyryl donor groups bearing short chiral *(S)*-2-methylbutyl chains in positions 4, 3,4 and 3,5, connected to electron-accepting 2,2-bipyrimidine rings, has been developed. Their linear and non-linear optical properties were studied using a variety of techniques, including one- and two-photon absorption spectroscopy, fluorescence measurements, as well as Hyper-Rayleigh scattering to determine the first hyperpolarizabilities. Their electronic and geometrical properties were rationalized by TD-DFT calculations. The thermal properties of the compounds were also investigated by a combination of polarized light optical microscopy, differential scanning calorimetry measurements and small-angle X-ray scattering experiments. The derivatives were found not to have mesomorphic properties, but to exhibit melting temperatures or cold crystallization behavior that enabled the isolation of well-organized thin films. The nonlinear optical properties of amorphous or crystalline thin films were studied by wide-field second harmonic generation and multiphoton fluorescence imaging, confirming that non-centrosymmetric crystal organization enables strong second and third harmonic generation. This new series confirms that our strategy of functionalizing 3D organic octupoles with short chiral chains to generate non-centrosymmetric organized thin films enables the development of highly second order nonlinear optical active materials without the use of corona-poling or tedious deposition techniques.

Introduction

Second Harmonic Generation (SHG) stands as a quintessential nonlinear optical process, captivating researchers with its unique properties and diverse applications such as spectroscopy, biological imaging, quantum computing and fiber-optic communication.[1] Originating from the interaction of photons within a nonlinear medium, SHG manifests itself as the generation of light at twice the frequency of the incident light, holding immense promises in various scientific domains spanning from material science to biology. This phenomenon, embedded within the realm of nonlinear optics, has garnered substantial interest, particularly in the context of thin film technologies.[2] The use of thin films of organic chromophores in nonlinear optics is also growing due to their ease of processing, versatility and tunability, and offers growing potential in optical communication, optical switching, frequency conversion and more.[3] Organic SHG thin films have in particular sparked considerable interest in data storage due to their potential for high-density information encoding.[4] SHG-based data storage exploits the nonlinear optical properties of thin film structures, enabling the creation of ultrahigh-density storage media with promising prospects for next-generation data storage technologies. As to this purpose non-centrosymmetric incorporation of organic chromophores into thin films is necessary. However, most of SHG-active organic thin films are achieved by using the corona-poling process, in which a strong electric field is applied to align dipolar organic chromophores inside a polymer matrix near its glass transition temperature (Tg).[5] Unfortunately, after cooling, most of these corona-poled SHG-active polymeric materials lack long-term stability and reproducibility of the preparation process, while the strong electric fields used during the corona-poling process can lead to degradation. The Langmuir-Blodgett technique has also been used to deposit non-centrosymmetric films using amphiphilic chromophores but the tedious monolayer-by-monolayer deposition method remains an obstacle.[6]

Recently, we have demonstrated that the proper functionalization of 3D octupolar chromophores can lead to the formation of non-centrosymmetric liquid crystalline thin films in which emerge strong SHG properties, competitive to inorganic crystalline materials as KH_2PO_4 (KDP) without any corona-poling process or tedious deposition technique. Indeed, the grafting of

[a] *P. Nicolas, Dr. O. Jeannin, Dr. N. Bellec, Prof. H. Akdas-Kiliç, Dr. F. Camerel*
Institut des Sciences Chimiques de Rennes CNRS-UMR 6226
Université de Rennes, Rennes, France
E-mail: franck.camerel@univ-rennes.fr

[b] *S. Abdallah, Prof. J.-P. Malval*
Institut de Science des Matériaux de Mulhouse CNRS-UMR 7361
Université de Haute Alsace, Mulhouse, France

[c] *A. Dok, Y. de Coene, Prof. T. Verbiest, Prof. K. Clays, Dr. S. Van Cleuvenbergen*
Department of Chemistry
Katholieke Universiteit Leuven, Leuven, Belgium

[d] *Prof. B. Bilgin-Eran, Prof. H. Akdas-Kiliç*
Department of Chemistry
Yildiz Technical University, Istanbul, Turkey
E-mail: hakdas@yildiz.edu.tr

Supporting information for this article is available on the WWW under https://doi.org/10.1002/asia.202400112

chiral 3,7-dimethyloctane carbon chains at the 3,4 positions of styryl groups attached to 2,2′-bipyrimidine, allows for the emergence of thermodynamically stable liquid crystal phases which can easily be proceeded into thin films. These liquid crystalline thin films present strong second harmonic generation resulting from the supramolecular organization of the chromophores into right or left-handed twisted columnar aggregates.[7] More recently, the only substitution of the 4 position by chiral 3,7-dimethyloctane sidechains on the styryl fragment has been investigated. Despite the absence of mesomorphic properties, non-centrosymmetric crystalline thin-film with strong SHG activity have nevertheless been obtained,[8] proving that our simple rational design strategy, i.e. grafting of chiral fragments on 3D octupoles, allows the emergence of non-centrosymmetric organization within processable crystalline or liquid crystalline (i.e. organized) thin films. These investigations into its structural modifications and incorporation into thin films show that bipyrimidine emerges as a promising candidate for the development of advanced SHG-active materials, representing significant perspectives toward the realization of efficient nonlinear optical devices and high-density data storage media.

In this context, we have investigated the impact of introducing shorter chiral chains at the periphery of the bipyrimidine bearing four divergent vinyl phenyl substituents on the thermal transitions, the optical properties, and the molecular organization. For this purpose, a new series of bipyrimidine functionalized with chiral *(S)*-2-methyl-butyl chains (C4(1)) in various positions have been developed (Scheme 1). The thermal properties of the bipyrimidine derivatives have been investigated by a combination of differential scanning calorimetry measurements and polarized optical microscopy observations. The molecular organization in the various states of matter was analysed by small angle X-ray diffraction and the one- and two-photons absorption and emission properties have been studied in solution and rationalized by DFT calculations. Finally, the SHG properties of these compounds isolated as thin films were studied in solid state using advanced laser measurement technologies. Depending on the alkoxy chain-substitution pattern on the compounds, the bipyrimidine derivatives exhibit distinctive thermal behaviours and NLO properties. We demonstrate that functionalizing 3D organic octupoles with short chiral chains modulates melting properties and can give rise to large-scale organized thin films that, combined with the symmetry breaking imported by chirality, exhibit strong second harmonic generation activity without the use of corona-poling or tedious deposition technique.

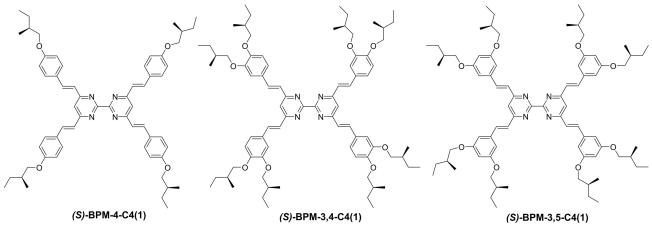

Scheme 1. Molecular structures of the studied chiral bipyrimidine based compounds.

Results and Discussion

Syntheses

The synthesis of the targeted compounds starts with the synthesis of 4,4′,6,6′-tetramethyl-2,2′-bipyrimidine (Me_4BPM) and of three alkoxybenzaldehydes substituted in the 4 or 3,4 or 3,5 positions by branched chiral *(S)*-2-methylbutyl chains. 4,4′,6,6′-tetramethyl-2,2′-bipyrimidine was freshly prepared *via* an Ullman-type coupling following a literature procedure from the commercial compound 2-chloro-4,6-dimethylpyrimidine compound.[9] The alkoxy-substituted benzaldehyde functionalized in 4[10] and 3,4 positions (compound **2** and **3** in scheme 2) were directly prepared from the corresponding hydroxybenzaldehyde by an alkylation reaction with *(S)*-1-iodo-2-methylbutane.[11] The commercial *(S)*-2-methylbutan-1-ol compound was converted into its iodo derivative to facilitate the alkylation reaction. 3,5-dihydroxybenzaldehyde is not commercially available, so the synthesis of compound **6** was carried out from methyl-3,5-dihydroxybenzoate which after alkylation with *(S)*-1-iodo-2-methylbutan was fully reduced with $LiAlH_4$ and oxidized with activated MnO_2 to get the corresponding aldehyde. The low reaction yield of 15% for the 3,4-di(*(S)*-2-methylbutoxy)benzaldehyde compound can be explained by the steric hindrance imported by the branched methyl group. For this reason, despite several attempts, the aldehyde functionalised in 3,4,5 positions have not been isolated. Full synthetic details are given in supporting information.

To obtain the targeted compounds of this new series, the final step is based on a synthetic route already reported in the literature and used for similar compounds.[12] Following the same procedure, ***(S)*-BPM-X–C4(1)** compounds have been synthesised by reacting 4,4′,6,6′-tetramethyl-2,2′-bipyrimidine with the corresponding aldehyde in NaOH 5 M in presence of Aliquat 336 (scheme 2). After purification, the three functionalized bipyrimidine compounds were isolated as yellow powders

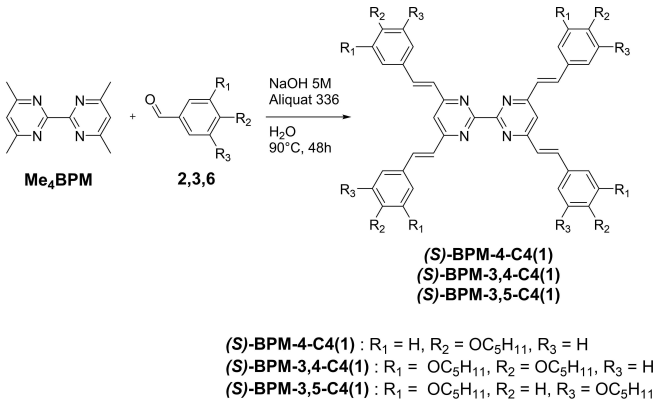

Scheme 2. Synthetic pathways used to obtain the targeted ***(S)*-BPM-X–C4(1)** compounds.

in good yields between 40–60%. The ^{1}H NMR investigations confirm the formation of the ethylenic bond with the appearance of two doublet systems at around 7.9 ppm and 7.2 ppm with a coupling constant of 16 Hz. Integration of all proton systems confirms that only tetrasubstituted compounds have been isolated (Figure S15–S20). Maldi-TOF spectrometry and elemental analysis further confirm the formation and the purity of the targeted compounds (see experimental part for full details).

Photophysical Properties in Solution

Figure 1 displays the one- (1PA) and two-photon (2PA) absorption spectra of the dyes as well as their respective fluorescence spectrum in solution in THF. Table 1 gathers the related spectroscopic data. For all derivatives, the low energy side of the 1PA spectrum exhibits a distinctive band in the 320–420 nm range whose position and intensity are both sensitive to the meta-to-para positioning of the alkoxy substituents. These spectral changes are particularly significant on going from the 3,5-disubstitued derivative to the 3,4-one for which the 1PA band is red shifted by about 22 nm concomitantly with an increase in intensity by ~20%. An additional absorption band of lower intensity is also observed around 300 nm, and its position is less sensitive to the substitution pattern.

In parallel, the fluorescence band of the 3,4 dye undergoes a strong bathochromic shift as compared to its 3,5 homologue (~51 nm) which leads to a significant stabilization of the lowest singlet excited state (S_1) of ***(S)*-BPM-3,4-C4(1)** (ΔE_{S1} ~0.27 eV). This S_1-level lowering clearly influences the emissivity of the 3,4 dye whose fluorescence quantum (Φ_f) is multiplied by more than one order of magnitude as compared to that of 3,5 one. This fluorescence 'switch-on' has been previously observed for similar alkoxy-based octupolar systems[12] and can be attributed to an efficient radiative process occurring from an intramolecular charge transfer state (^{1}ICT). Indeed, this emissive state involves a charge transfer from the alkoxy donor groups to the bipyrimidine electron-acceptor core associated with a long-range electronic delocalisation along the stilbenyl branches which play the role of π-electron relays. It is worth noting that the radiative rate constants (k_r) of the two derivatives in the 4 position display comparable values in the 0.2–0.3×10^9 s^{-1} range suggesting an equivalency for the electronic configuration of their emissive ^{1}ICT state. By contrast, this electronic configuration is clearly different for the 3,5 component whose k_r is divided by a factor ~5.5 confirming thereby the reduction of the ICT character of the emissive state. This shows the predominant effect of the stronger mesomeric effect in the 4

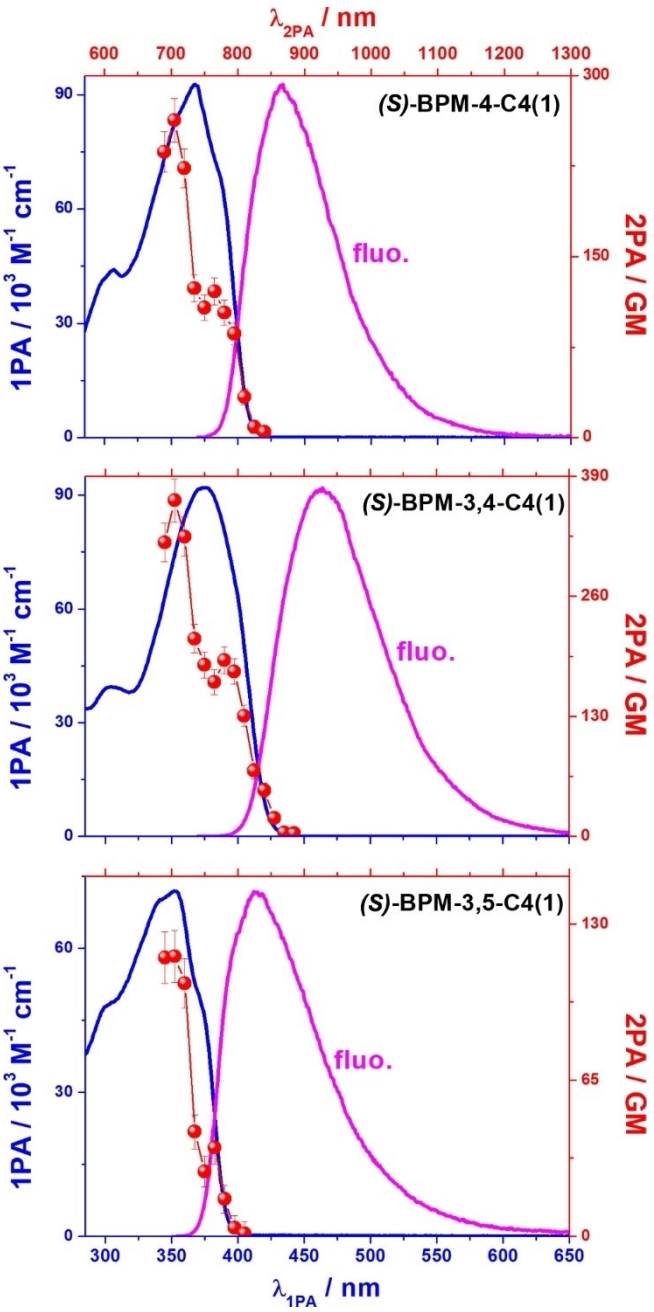

Figure 1. 1PA (blue lines), 2PA (red circles) and fluorescence spectra of chromophores in THF.

Table 1. One- and Two-Photon Spectroscopic data of compounds in **THF**.

	ε_{abs} ($M^{-1}cm^{-1}$)	λ_{1P} (nm)	λ_{fluo} (nm)	E_{00}[a] (eV)	Φ_{fluo}	τ_{fluo}[b] (ns)	k_r[c] (10^9 s^{-1})	k_{nr}[c] (10^9 s^{-1})	$\frac{k_{nr}}{k_r}$	λ_{2P} (nm)	δ_{2P}[d] (GM)
(S)-BPM-4-C4(1)	92610	369	433	3.12	0.09	0.31	0.29	2.94	10.1	705	264
(S)-BPM-3,4-C4(1)	91900	375	465	2.99	0.36	1.65	0.22	0.39	1.8	705	365
(S)-BPM-3,5-C4(1)	71860	353	414	3.26	0.03	0.69	0.04	1.41	35.3	690	116

[a] $E_{00} \approx {}^1/_2\, hc(\nu_{abs}+\nu_{fluo})$ [b] Average fluorescence lifetime from a bi-exponential fit [c] $k_r = \Phi_{fluo}/\tau_{fluo}$ and $k_{nr} = (1-\Phi_{fluo})/\tau_{fluo}$ [d] The uncertainty in δ is ±15%.

position in ***(S)*-BPM-4-C4(1)**; further enhanced by a smaller inductive effect in ***(S)*-BPM-3,4-C4(1)**; but absent in the ***(S)*-BPM-3,5-C4(1)**.

It clearly appears that the isomerism of the alkoxy groups mainly drives the efficiency of the ICT process within each D-π-A branch of the octupoles. This structural effect also affects the two-photon absorption (2PA) performances of the derivatives. As shown in Figure 1, all the 2PA spectra have similar shape with two distinctive bands: a weakly intensive band located in the 740–900 nm range and a more intensive one in the high energy region with a maximum at ~690 nm for the meta-meta derivative and at ~705 nm for the para-substituted dyes. The 2PA spectra do not coincide with their corresponding 1PA ones. This spectral effect has been previously observed for similar bipyrimidine-based octupoles with alkoxystyryl groups[8,12] and should be assigned to the near D2d centrosymmetry of these octupoles series resulting in a theoretically two-photon forbidden character of their S0→S1 transition.[13,14,15] Therefore the mainly active 2PA band in the high energy region should be assigned to a high-lying S0→Sn transition. As expected, the corresponding maximum 2PA cross-section (λ_{MAX}) is notably amplified by a factor ~3 upon substitution in the 4 position confirming an enhancement of the ICT character within this two-photon active S0→Sn transition.

Hyper-Rayleigh Scattering (HRS) was employed to determine the second-order nonlinear optical properties of these chirally substituted bipyrimidines (Table 2). HRS experiments were performed in chloroform at 1300 nm. This wavelength was selected for comparison with the earlier measurements, and with the aim to avoid multiphoton fluorescence (MPF) contribution to the HRS signal. Such MPF contributions have been observed and dealt with in the earlier reports, either with active MPF suppression and the determination of a fluorescence lifetime in the frequency domain[7,12] or with discrimination between a narrow HRS peak on a broad MPF background in the spectral domain.[8] The same experimental procedure was used as reported in these earlier works. The experimentally derived dynamic hyperpolarizability value at 1300 nm ($\beta_{HRS,1300}$) as well as the static value, calculated from that dynamic value by applying the undamped three-level model for octupoles ($\beta_{HRS,o}$), are reported for comparison with the earlier reported values for similar bipyrimidines with a slightly different substitution pattern.[7,8,12]

Table 2. Hyperpolarizability values in chloroform.

	$\beta_{HRS,1300}$ (10^{-30} esu)	$\beta_{HRS,o}$ (10^{-30} esu)
(S)-BPM-4-C4(1)	220+/−40	130+/−20
(S)-BPM-3,4-C4(1)	N.D.	/
(S)-BPM-3,5-C4(1)	160+/−15	100+/−8

$\beta_{HRS,1300}$: dynamic first hyperpolarizability at 1300 nm; $\beta_{HRS,o}$: static first hyperpolarizability derived from the (undamped) three-level model for octupoles with the resonance wavelengths (λ_{abs}) from table 1. ND: not possible to determine from the overwhelming MPF contribution to the HRS signal.

Within this series, the MPF contribution (broad spectral background) to the HRS signal (narrow peak at the second-harmonic wavelength only on top of that broad background) was too large for ***(S)*-BPM-3,4-C4(1)**, which was already characterized as the one with the most red-shifted absorption and emission spectrum and the largest two-photon absorption coefficient, all congruent with the mesomeric advantage of the para-substitution by a donating group, reinforced by the inductive effect of an additional donor. Note that from the apolar nature of the tetrasubstituted bipyrimidine, only HRS is capable of experimentally providing a value for the first hyperpolarizability. Electric-field-induced Second-Harmonic Generation (EFISGH) is not appropriate as the octupolar chromophore with D2 topology does not possess a dipole moment for the static electric field to interact with.

For both ***(S)*-BPM-4-C4(1)** and ***(S)*-BPM-3,5-C4(1)**, a value was obtained that is a little bit larger than the earlier reported first hyperpolarizability values (static value derived from the three-level model for octupoles $\beta_{HRS,o}$ between 38+/−8 and 66+/−15),[7,8,12] but still in line with what can be expected from the octupolar bipyrimidine core. The somewhat larger value is attributed to the presence of the chiral substituent(s) that add non-zero off-diagonal hyperpolarizability tensor components (e.g.βijk) to that third-rank tensor, so that the total β_{HRS} increases.

When comparing ***(S)*-BPM-4-C4(1)** and ***(S)*-BPM-3,5-C4(1)**, the smaller $\beta_{HRS,o}$ value is then obtained for ***(S)*-BPM-3,5-C4(1)**, which lacks the beneficial para-substitution, as is already discernible in the blue-shifted absorption and emission spectrum and the smallest two-photon absorption coefficient. Note how this small MPF contribution to the HRS signal shows as the smaller estimate for experimental uncertainty on the retrieved value.

DFT Calculations

To better understand the electronic properties and geometries of ***(S)*-BPM-X–C4(1)** compounds, DFT geometrical optimizations were performed in vacuum starting from a planar conformation or a conformation in which the two pyrimidine moieties are at 90°. Theoretical calculations were performed using Gaussian 16 software with the DFT/B3LYP method and a 6-31G++ basis set.[16] The geometric structures were optimized in a convergent process by minimizing the energy of the conformations for all geometric parameters until a new structure with minimum energy was obtained. The stability of all optimized compounds was confirmed by the absence of imaginary frequencies. The optimized geometrical structures were drawn and analyzed using GaussView.[17] After optimization, the planar molecule remains in a flat conformation for ***(S)*-BPM-4-C4(1)** and ***(S)*-BPM-3,4-C4(1)**. Starting with a 90° angle, the twisted molecule converges to a conformation with a dihedral angle between the two pyrimidine fragments of 44.70°and 42.81° for ***(S)*-BPM-4-C4(1)** and ***(S)*-BPM-3,4-C4(1)**, respectively. The energy difference between the two conformations is only 0.04 eV for each molecule, meaning that both pyrimidine fragments can easily

rotate around the central C–C bond (Figure SI.21). Indeed, crystal structures obtained on similar bipyrimidine compounds have demonstrated that the two pyrimidine fragments can easily rotate around the central C–C bond with a dihedral angle which can vary from 0 to 70°.[18] It should be noted, however, that the planar conformation in the solid state, with a dihedral angle of 0°, was only observed when the two pyrimidine fragments were hydrogen-bonded to a methanol molecule. Furthermore, total energy calculations show that the twisted conformation is slightly more stable. Thus, the molecule certainly adopts a D2 topology rather than a D4 topology in solution and in solid state. The introduction of alkoxy chains in positions 3 and 5 on ***(S)*-BPM-3,5-C4(1)** compound imports certain steric constraints that hinder the planar conformation and the molecule is finally optimized with a dihedral angle of 46.18° between the two pyrimidine fragments. Starting from an angle of 90°, the twisted molecule also converges to a conformation with a dihedral angle between the two pyrimidine fragments of 45.32°. These calculations show that the ***(S)*-BPM-3,5-C4(1)** compound can therefore hardly adopt a planar conformation. Note that in all cases, the bis(styryl)-pyrimidine fragments are completely flat, in line with a good electron delocalization along the half-molecule.

Figure 2 shows the calculated HOMO and LUMO levels of each molecule in the twisted conformation, which is the conformation most commonly observed in the crystalline and liquid-crystalline phases. Examination of the nature of the frontier molecular orbitals of the calculated models shows that HOMO is mainly centered on the alkoxy-styryl branches, while LUMO is mainly centered on the bipyrimidine fragment, confirming the charge-transfer character of the HOMO-LUMO transition. The introduction of alkoxy chains in the meta position decreases the energy of the LUMO levels, while the introduction of alkoxy chains in the para position increases the energy of the HOMO levels. The HOMO-LUMO gap is higher for the 3,5 substitution pattern, with a value of 3.65 eV. Substitution at position 4 in compound ***(S)*-BPM-4-C4(1)** induces a greater decrease in the HOMO-LUMO transition at 3.55 eV, in agreement with the red shift observed in the UV absorption spectrum. This confirms that the donor effect is greater in the para position than in the meta position. The lowest HOMO-LUMO gap is obtained with the introduction of alkoxy chains in position 3,4 in the ***(S)*-BPM-3,4-C4(1)** compound, consistent with the observation of an even more red-shifted absorption band on the UV-vis spectrum.

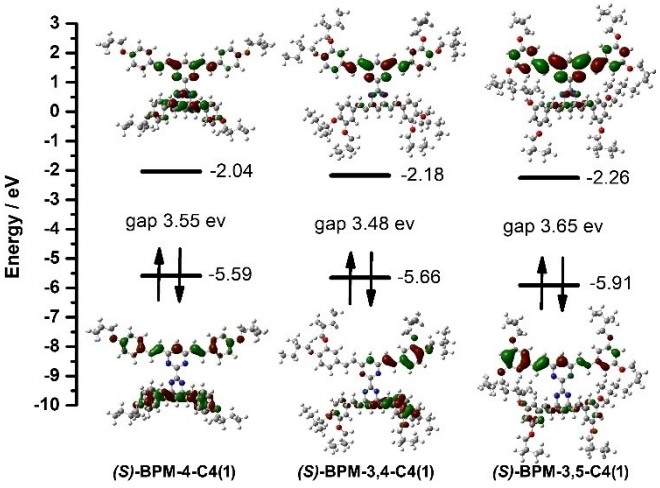

Figure 2. Frontier orbitals with energy levels (eV) of the ***(S)*-BPM-C4(1)** compounds obtained by DFT B3LYP/6-31 + + (isovalue of 0.03 [e bohr^{-3}]$^{1/2}$) (HOMOs and LUMOs are degenerated into several close-energy orbitals, and only higher-energy HOMO level and lower-energy LUMO level are shown).

TD-DFT calculations over 40 excited states performed on the optimized twisted ***(S)*-BPM-4-C4(1)** compound confirm that the compound displays two absorption bands between 250 and 400 nm (Figure S22). The low energy absorption band around 380 nm is associated to electronic π–π* transitions from the alkoxystryryl arms to the central bipyrimidine electron acceptor. The highest-energy absorption band around 300 nm is associated with a combination of π–π* transitions and n–π* electronic transitions from the nitrogen doublets to empty π* orbitals centred on the bipyrimidine fragment (Table S1).

Thermal Behaviours and Thin Films Organizations

The thermal properties of the various BPM compounds were studied by combining polarized-light optical microscopy (POM) observations and differential scanning calorimetry (DSC) measurements, whereas the molecular organizations in the various phases were analysed by small-angle X-ray scattering (SAXS) experiments.

The pristine ***(S)*-BPM-4-C4(1)** compound appears as an amorphous solid between crossed polarizers (Figure S23a). Upon heating, around 200 °C, the compound clearly starts to crystallize as attested by the apparition of highly birefringent solid needles. The coexistence of crystalline and amorphous domains persists until the melting transition detected between 250 and 260 °C. Above 260 °C, ***(S)*-BPM-4-C4(1)** compound is an isotropic liquid state and appears completely dark under crossed polarizers (Figure S23c). After cooling at room temperature, the compound remains in an amorphous state, hardly deformable under gentle pressure on the glass cover-slide (Figure S23d). DSC traces confirm that this compound undergoes clear cold crystallization. Cold crystallization occurs upon heating when the molecules gain sufficient mobility to arrange themselves into an ordered structure. The heating curves show a broad exothermic peak between 180 °C and 250 °C which is attributed to the slow crystallization of the compound upon heating, directly following by a sharper endothermic peak attributed to the melting of the crystalline phase into an isotropic liquid. A weak reversible glass transition centred at 110 °C is also observed and indicates that the compound transits from a solid amorphous state to an isotropic liquid around this temperature. SAXS measurements unambiguously confirm the cold crystallization of the compound upon heating. The SAXS patterns recorded upon the second heating are presented in Figure 3. Below 180 °C, the XRD patterns display two broad diffraction peak at 4 and 20° in 2θ, corresponding to the mean intermolecular distance and to the mean distance

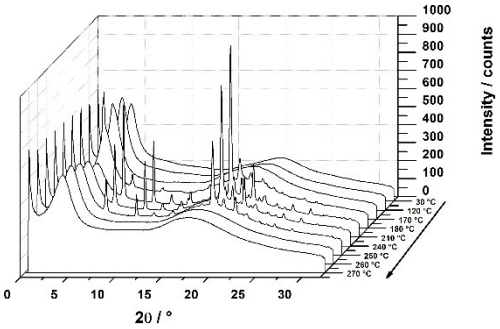

Figure 3. Temperature-dependent SAXS patterns recorded upon heating on ***(S)*-BPM-4-C4(1)** compound.

between the carbon chains, respectively. These XRD patterns are typical of amorphous compounds. Between 180 and 260 °C, the SAXS patterns display several sharp diffraction peaks in the small and wide angles regions, confirming the crystallization of the compounds in this temperature range. The reminiscence of a broad diffusion halo at 4° in 2θ indicates partial and incomplete crystallization of the compound, as observed in POM images where the coexistence of an amorphous and a crystalline phase can be observed up to the melting point (Figure S23b). Finally, above 260 °C, the SAXS pattern are again characteristic of an amorphous compound, with only two broad diffusion halos visible on the SAXS patterns. Thus, with ***(S)*-BPM-4-C4(1)** compound, only amorphous thin films can be isolated at room temperature after complete melting.

The DSC of the ***(S)*-BPM-3,4-C4(1)** compound is simpler, with a single reversible thermal transition centred at 188 °C. POM observations shows that below 188 °C, the compound is in a crystalline state as attested by the presence of large birefringent spherulites (Figure 4b), whereas above 188 °C, the compound is clearly in an isotropic fluid state (Figure 4a). The transition is thus attributed to a direct melting of a crystalline compound into an isotropic fluid. SAXS measurements performed on heating and cooling confirms this attribution. SAXS patterns recorded below 188 °C are all characteristic of a crystalline phase with several sharp diffraction peaks in the whole 2θ range explored. On the other hand, SAXS diagrams recorded above 188 °C, show only broad diffusion halos corresponding to mean intermolecular distances.

Compound ***(S)*-BPM-3,4-C4(1)** is deprived of mesomorphic properties and only crystalline thin films can be isolated at room temperature.

Like the ***(S)*-BPM-4-C4(1)** compound, the ***(S)*-BPM-3,5-C4(1)** compound undergoes a clear cold crystallization upon heating as confirmed by the presence of an exothermic peak on the DSC heating curves at 100 °C (Figure 5). However, unlike compound ***(S)*-BPM-4-C4(1)**, the crystalline phase persists over a wider temperature range from 100 °C to melting, which begins at around 191 °C. POM observations confirm that the compound fully crystallized above 100 °C with the appearance of a pseudo-fan shaped texture hardly deformable under gentle pressure on the glass cover slide (Figure 6a). SAXS patterns recorded between 100 °C and 175 °C with several sharp

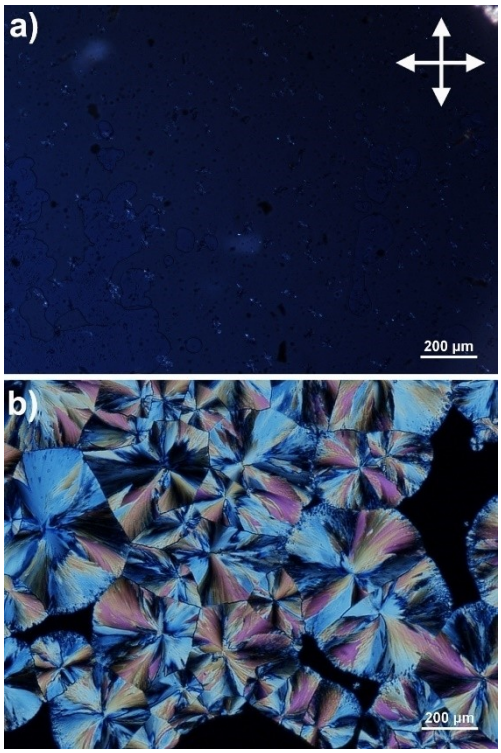

Figure 4. Optical photomicrograph of the ***(S)*-BPM-3,4-C4(1)** compound obtained with a polarizing microscope at 250 °C (a) and at 165 °C (b) upon cooling from the isotropic state (crossed-polarizers symbolized by the white cross in the corner of the picture).

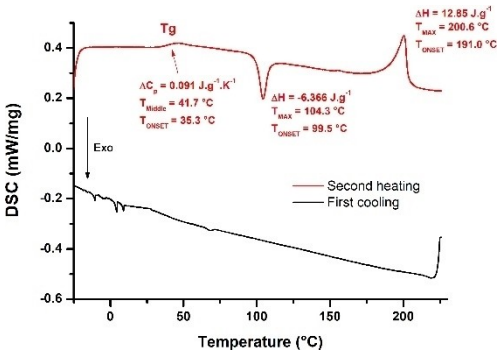

Figure 5. DSC traces of the ***(S)*-BPM-3,5-C4(1)** compound (scan rate: 10 °C/min; small peaks on the cooling curve below 25 °C are measurement artefacts).

diffraction peaks over the whole 2θ range are all characteristic of a highly organized phase (Figure 7). Above the high temperature endothermic peak centred at 201 °C, the compound is in an isotropic state, as confirmed by POM with the observation of a fluid and non-birefringent phase between crossed polarizers (Figure 6b). The SAXS patterns recorded in the isotropic state display only broad diffusion halos attributed to mean intermolecular distances in the fully disordered state (Figure 7). Upon cooling from the isotropic state, the compound remains in an amorphous state down to room temperature, as confirmed by SAXS analysis and POM observations. This compound therefore has no mesomorphic properties either, and only a crystalline

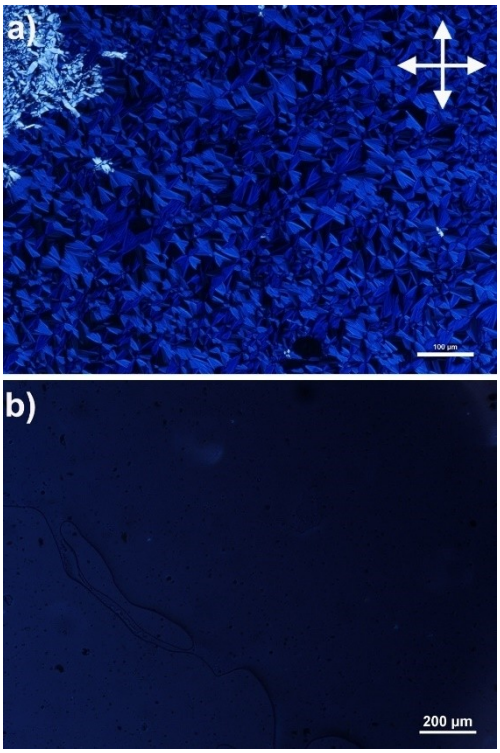

Figure 6. Optical photomicrograph of the ***(S)*-BPM-3,5-C4(1)** compound obtained with a polarizing microscope at 150 °C (a) and at 250 °C (b) upon heating (crossed-polarizers symbolized by the white cross in the corner of the picture).

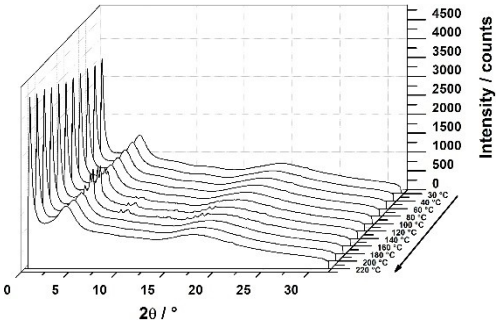

Figure 7. SAXS patterns recorded on the ***(S)*-BPM-3,5-C4(1)** compound upon heating from 30 °C to 220 °C.

phase is formed between 100 °C and 191 °C on heating. The weak glass transition detected only on heating around 42 °C, prior to cold crystallization, allows the molecules to acquire sufficient mobility to crystallize. On cooling, from the isotropic state, only amorphous thin films can be isolated, but we have found that the crystalline phase and its texture, obtained on heating, can be frozen at room temperature by rapid cooling. SAXS analyses confirm that the crystalline phase generated between 100 and 175 °C can be isolated at room temperature after cooling (Figure S27). This thermal treatment can therefore also be used to isolate homogeneous crystalline thin films at room temperature (*vide infra*).

All these new compounds with a short chiral chain lack mesomorphic properties, but after heat treatment they can be used to isolate amorphous or crystalline chiral thin films. While ***(S)*-BPM-4-C4(1)** compound allows to isolate amorphous thin films and ***(S)*-BPM-3,4-C4(1)** compound crystalline thin films at room temperature, ***(S)*-BPM-3,5-C4(1)** allows to isolate both amorphous and crystalline films depending on the heat treatment applied.

Non-linear Optical Properties in Solid State

The nonlinear optical properties in the solid state were interrogated through widefield multiphoton microspectroscopy (MPF) at a wavelength of 1024 nm, employing a setup described elsewhere. All experiments were conducted at room temperature. The emergence of a strong SHG response critically relies on achieving noncentrosymmetry in the bulk. In our previous studies, we demonstrated the ability to induce SHG activity in solid-state bipyrimidine compounds.[7,8,12] This induction is achieved by substitution with chiral side chains, as enantiomerically pure materials are by default non-centrosymmetric. However, this molecular design strategy necessitates an efficient transfer of molecular chirality to supramolecular chirality. For compound ***(S)*-BPM-4-C4(1)** however, only amorphous thin films could be isolated at room temperature after complete melting. Hence, in this case, the molecular chirality was not efficiently transferred to the bulk, as evidenced by the absence of a measurable SHG signal (Figure 8). In fact, a weak signal was detectable in the SHG channel, but a spectroscopic measurement revealed that this was due to a contribution of

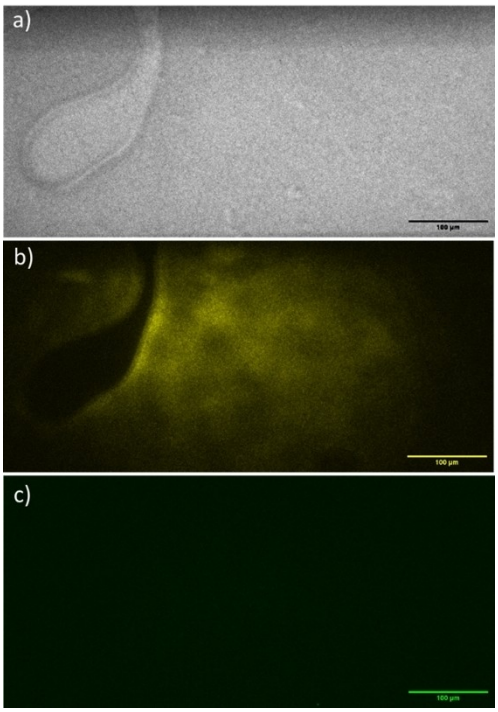

Figure 8. Recorded images of compound ***(S)*-BPM-4-C4(1)**. a) Brightfield image of compound ***(S)*-BPM-4-C4(1)** illuminated through a LED source. Recorded MPF (b) and SHG (c) image of compound ***(S)*-BPM-4-C4(1)** with an incoming s-polarized laser source at a beam intensity of 210 mW.

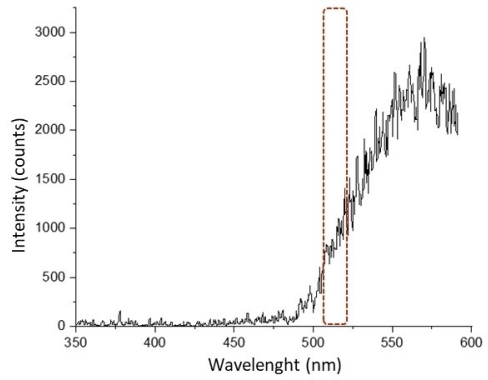

Figure 9. Obtained spectrum of compound ***(S)*-BPM-4-C4(1)** show no indication of SHG signal at 512 nm (red dashed box). The spectrum was from an incoming s-polarized laser source with an intensity of 159 mW.

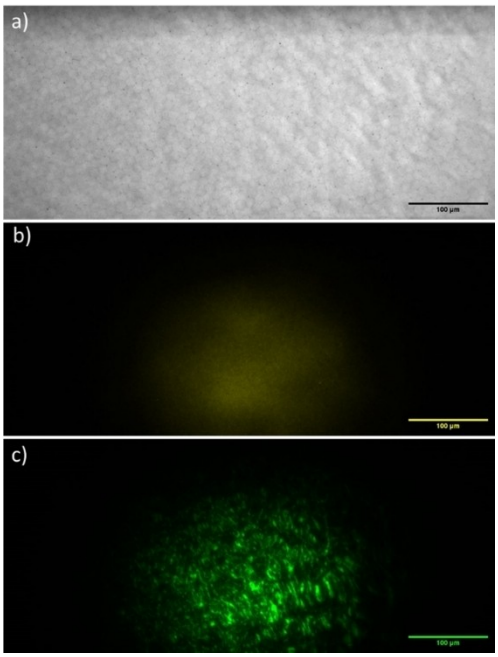

Figure 10. Recorded images of compound ***(S)*-BPM-3,4-C4(1)**. (a) Brightfield image of compound ***(S)*-BPM-3,4-C4(1)** illuminated through a LED source. Recorded MPF (b) and SHG (c) image of compound ***(S)*-BPM-3,4-C4(1)**. The MPF image was obtained at a laser beam power of 150 mW, while for SHG image an incoming laser beam intensity of 33 mW was sufficient.

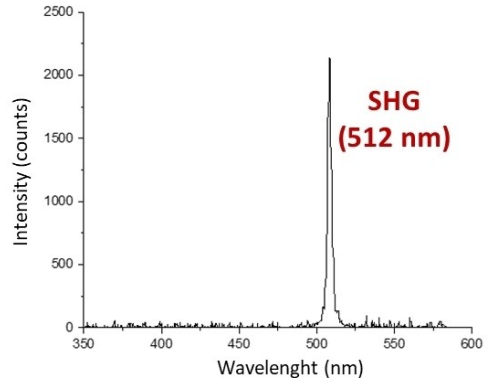

Figure 11. Spectrum obtained for compound ***(S)*-BPM-3,4-C4(1)**. The power of the incoming laser beam was kept at 10 mW.

multiphoton fluorescence (MPF) at the same wavelength (indicated in red) (Figure 9). Unlike SHG, MPF does not rely on noncentrosymmetric organization. The relatively weak MPF response in the solid state can be attributed to aggregation induced quenching. For compound ***(S)*-BPM-3,4-C4(1)**, it was possible to isolate the crystalline phase at room temperature upon cooling from the isotropic phase. While the texture is not immediately evident from the optical image, the SHG image clearly reveals a polycrystalline film with non-centrosymmetric (chiral) organization (Figure 10). A weak multiphoton fluorescence background is present here as well, but is clearly overpowered by the strong SHG signal, which appears already at much lower laser power. This is further confirmed by a spectroscopic measurement shown in Figure 11, demonstrating the dominant nature of the SHG. Finally, for the compound ***(S)*-BPM-3,5-C4(1)**, a fully crystalline thin film could be isolated at room temperature by rapid cooling of the crystalline phase formed during heating to 150 °C. This approach allowed us to isolate the pseudo-fan shaped texture of the crystalline state (Figure 12). In this case, the texture is readily picked up by the optical image and SHG imaging confirms the non-centrosymmetric (chiral) organization of the polycrystalline film, also here accompanied by a weak MPF signal. The texture observed under crossed polarizers could be remarkably observed by SHG, confirming that the SHG signal is strongly correlated to molecular organization and orientation within the thin film. This observation is further supported by a spectroscopic measurement, which also displays a peak at 343 nm, corresponding to third-harmonic generation (see Figure13). Overall, our experiments demonstrate the significant impact of molecular and supramolecular chirality on the SHG activity in solid-state bipyrimidine-based compounds.

Conclusions

A series of bipyrimidine-based chromophores featuring alkoxystyryl donor groups bearing chiral *(S)*-2-methylbutyl chains in positions 4, 3,4 and 3,5 has been developed. The photophysical studies in solution revealed that the introduction of an alkoxy fragment in the para-position induces a red-shift of the absorption band and strongly enhances the luminescence

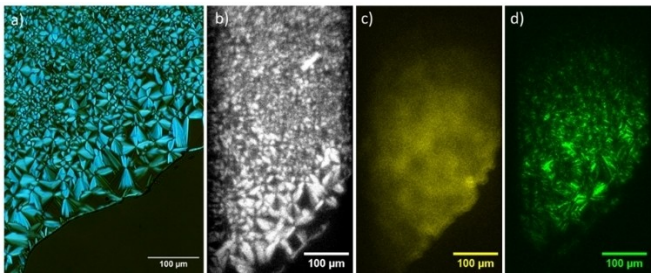

Figure 12. Polarized optical image of compound ***(S)*-BPM-3,5-C4(1)** obtained through optical microscope (a). Polarized bright field image obtained with a polarized LED source recorded on the iCCD camera (b). MPF (c) and SHG (d) images illuminated with an incoming s-polarized laser source at a laser power of 510 mW.

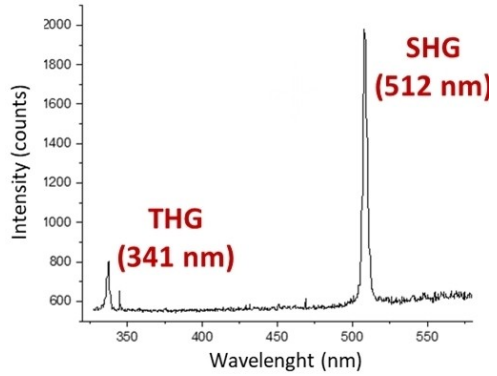

Figure 13. Spectrum obtained for compound ***(S)*-BPM-3,5-C4(1)**. The sample was illuminated with a laser source with an intensity of 510 mW. The spectrum shows clear SHG and THG signal.

properties and the 2PA cross-section. Consequently, due to a strong MPF contribution, the first hyperpolarizability values could not be determined for the compound ***(S)*-BPM-3,4-C4(1)** by HRS measurements. For the less luminescent compounds ***(S)*-BPM-4-C4(1)** and ***(S)*-BPM-3,5-C4(1)**, the first hyperpolarizability values were obtained and are somewhat larger than previously reported values for similar compounds. DFT geometrical optimization have shown that the molecule adopts a twisted conformation with a dihedral angle around 45°. Especially, the ***(S)*-BPM-3,5-C4(1)** compound cannot adopt a planar conformation due to the steric constraints imported by the substitution in the 3,5 positions. Analysis of the energy frontier orbitals supported that the para substitution induces a stronger donor effect than the meta substitutions and TD-DFT calculations have confirmed that the strong absorption at around 380 nm is attributed to π–π^* charge transitions from the alkoxystyryl arms to the central bipyrimidine electron acceptor core. The thermal properties of the compounds were investigated by a combination of POM observations, DSC measurements and SAXS analysis. All compounds are devoid of mesomorphic properties. For compound ***(S)*-BPM-4-C4(1)**, cold crystallization was observed on heating, but due to instant melting in the isotropic phase, only amorphous or biphasic thin films could be isolated at room temperature. Compound ***(S)*-BPM-3,5-C4(1)** also undergoes cold crystallization, but the clear separation between crystallization and melting on heating enables crystalline thin films to be easily frozen at room temperature by rapid cooling. Such compounds, which undergo cold crystallization, can be of great interest to be used as heat storage materials.[19] Finally, ***(S)*-BPM-3,4-C4(1)** compound simply displays a reversible melting transition which permitted to directly isolate crystalline thin films at room temperature on cooling from the isotropic fluid phase. SHG activity in solid-state bipyrimidine compounds has been investigated through wide-field multiphoton microspectroscopy at a wavelength of 1024 nm. Measurements performed on the amorphous thin films and on the crystalline thin films have confirmed that SHG signal only emerged from organized materials. No SHG signal could have been detected on the amorphous thin films of ***(S)*-BPM-4-C4(1)** compound whereas strong SHG and even THG signal could easily be detected on crystalline thin films of ***(S)*-BPM-3,4-C4(1)** or ***(S)*-BPM-3,5-C4(1)** compounds. These measurements confirmed that the organization of chiral octupolar molecules into crystalline thin films allows for the generation of strong higher harmonic signal. These new results series confirm that our strategy of functionalizing 3D organic octupoles with chiral chains to generate non-centrosymmetric organized thin films (crystal or liquid crystal) enables the development of highly SHG-active materials without the use of corona-poling or tedious deposition techniques. This work paves the way for the development of advanced SHG-active materials, which can be of great interest for nonlinear optical devices and high-density data storage media.

Supporting Information

Full synthetic details and characterizations of the bipyrimidine compounds with ^{1}H and ^{13}C NMR spectra. Representation of the DFT geometry-optimized molecular structures of ***(S)*-BPM-C4(1)** compounds starting from a planar conformation or a 90° twisted conformation. Energy and composition of the first singlet excited states and UV-visible absorption spectra of the optimized twisted ***(S)*-BPM-4-C4(1)** compound simulated by TD-DFT calculation. Additional DSC (***(S)*-BPM-4-C4(1)** and ***(S)*-BPM-3,4-C4(1)**), POM (***(S)*-BPM-4-C4(1)**) and X-rays analyses (***(S)*-BPM-3,4-C4(1)** and ***(S)*-BPM-3,5-C4(1)**). Cartesian coordinates of all the ***(S)*-BPM-C4(1)** compounds after geometrical optimization.

Experimental Part

300 (^{1}H) and 75.5 MHz (^{13}C) NMR spectra were recorded on Bruker Avance 300 spectrometer at room temperature using residual proton solvents as internal standards. FT-IR spectra were recorded using a JASCO ATR-FTIR 4100 spectrometer equipped with an ATR apparatus. Elemental analyses were performed by the Service de Microanalyse BioCIS, Faculté de pharmacie, Université Paris-Saclay, Orsay, France. Mass spectra were recorded with a MALDI-TOF Microflex LT Bruker.

Differential scanning calorimetry (DSC) was carried out by using NETZSCH DSC 200 F3 instrument equipped with an intracooler. DSC traces were measured at 10 °C/min down to −25 °C.

Optical microscopy investigations were performed on a Nikon H600 L polarizing microscope equipped with a Linkam "liquid crystal pro system" hotstage LTS420. The microscope is also equipped with a UV irradiation source (Hg Lamp, λ = 340-380 nm) and an ocean optic USB 2000+ UV-Vis-NIR spectrophotometer based on CCD detection technology.

X-ray scattering experiments (SAXS) were performed using a FR591 Bruker AXS rotating anode X-ray generator operated at 40 kV and 40 mA with monochromatic Cu Kα radiation (λ = 1.541 Å) or a XENOCS GeniX3D low convergence copper micro source (50 W) equipped with FOX3D single reflection optics and point collimation. The patterns were collected with a Mar345 Image-Plate detector (Marresearch, Norderstedt, Germany). The samples were held in Lindeman glass capillaries (1 mm diameter). The capillaries were placed inside a Linkam HFX350-Capillary X-Ray stage which allow measurements from −196 °C up to 350 °C with an accuracy of 0.1 °C.

The two-photon absorption (2PA) measurements were performed with femtosecond mode-locked laser pulse using a Ti: Sapphire laser (Spectra-Physics, Mai Tai: pulse duration: ~100 *fs*; repetition rate: 80 MHz; wavelength range: 690–1040 nm). A relative two-photon excited fluorescence method[20] was employed to measure the two-photon absorption cross-sections, δ. The measurements of 2PA cross-sections were performed relative to reference molecules (*r*) such as fluorescein[21,22,23] in water at pH = 11. The value of δ for a sample (*s*) is given by:

$$\delta_S = \frac{S_S \Phi_r \eta_r c_r}{S_r \Phi_S \eta_S c_S} . \delta_r$$

Where *S* is the detected two-photon excited fluorescence integral area, *c* the concentration of the chromophores, and Φ is the fluorescence quantum yield of the chromophores. η is the collection efficiency of the experimental set-up and accounts for the wavelength dependence of the detectors and optics as well as the difference in refractive indices between the solvents in which the reference and sample compounds are dissolved. The measurements were conducted in a regime where the fluorescence signal showed a quadratic dependence on the intensity of the excitation beam, as expected for two-photon induced emission. For the calibration of the two-photon absorption spectra, the two-photon excited fluorescence signal of each compound was recorded at the same excitation wavelength as that used for standards. The laser intensity was in the range of 0.2–2×10^9 W/cm^2. The experimental error on the reported cross section is 15%.

The absorption measurements were carried out with a Perkin Elmer Lambda 2 spectrometer. Steady-state fluorescence spectra in solution were collected from a FluoroMax-4 spectrofluorometer. Emission spectra are spectrally corrected, and fluorescence quantum yields include the correction due to solvent refractive index and were determined relative to quinine bisulfate in 0.05 molar sulfuric acid (Φ = 0.52).[24]

The fluorescence lifetimes were measured using a Nano LED emitting at 372 nm as an excitation source with a nano led controller module, Fluorohub from IBH, operating at 1 MHz. The detection was based on an R928P type photomultiplier from Hamamatsu with high sensitivity photon-counting mode. The decays were fitted with the iterative reconvolution method on the basis of the Marquardt/Levenberg algorithm.[25] Such a reconvolution technique allows an overall-time resolution down to 0.2 ns. The quality of the exponential fits was checked using the reduced χ^2 ($\leq$ 1.2).

For Hyper-Rayleigh scattering measurements, a custom designed optical setup was used to determine the first hyperpolarizabilities of the compounds. The laser (Insight DS+, Spectra-Physics) allows for a tunable output between 680 and 1300 nm. The former delivers femtosecond (~120 fs) pulses at an 80 MHz repetition rate. The output beam ($1/e^2 < 1.2$ mm) has a gaussian profile ($M_2 < 1.1$) is horizontally polarized (the plane of the optical table). A combination of an achromatic half-wave plate and Glan-Laser polarizer allows to control the output power in accordance to Malus's law. The polarizer is placed in such a way that the extraordinary ray is vertically polarized. The average power which is sent into the sample typically ranges from 500 to 1000 mW. The beam is routed to the input lens (aspheric, f = 8.00 mm) by a series of mirrors. A long pass filter with a cut-off at 690 nm is used to prevent any higher harmonic generation from the laser or the optics from entering the sample. The quartz cuvette (10x4 mm) is placed in a custom translation mount which allows to define the path length of the focal point relative to the side walls. Light is collected at 90° by an achromatic, aspheric condenser lens (f = 30 mm). The collimated beam passes a series of three large broadband dielectric elliptical mirrors to rotate the image 90°. The latter ensures maximal resolution of the spectrograph (vertically oriented slit). The collimated beam is focused on the spectrograph (IS/SM 500, Bruker) with a plano-convex lens, matching the focal length of the spectrograph (f = 200 mm, f/8). A blocking edge filter (FF01-720/SP-25, Semrock) ensures high optical density in the laser excitation range. One of two gratings (50 grooves/mm, 600 nm blaze or 150 grooves/mm, 500 nm blaze) were used, depending on the desired resolution, diffraction range and spectral profile of multiphoton emission spectra. An EMCCD camera (Ixon Ultra 897, Andor Solis) was used to image the spectra.

For NLO imaging, the sample was illuminated wide field under normal incidence with femtosecond pulsed infrared (IR) laser light at 1030 nm (Pharos, Light Conversion). The intensity and polarization of the incident IR light is varied by a combination of a zero-order half-wave plate for 1030 nm mounted in a computer-controlled rotation stage (Thorlabs, PRM-Z8) and a Glan-Taylor polarizer selecting for S-polarized light. The sample is irradiated by a long focal length lens (f = 5 cm) which is focused above the sample, so that the incident fundamental light can be considered to a good approximation as a collimated beam and electric field components along the propagation direction (Z) can be neglected. Behind the sample, a 20x objective (Nikon, CFI Plan Fluor 20X CH) collects the light. In the infinity path an IR filter rejects the laser light and a filter wheel selects the transmitted wavelength for SHG (Bandpass, 515 nm, Edmund Optics #65-153), MPF (Longpass, Cut-off wavelength 525 nm, Edmund Optics #84-744) or Bright field (no filter). A 20 cm tube lens (Mitutoyo) then images the light onto the slit of an imaging spectrometer (Andor, Kymera 328i), coupled to an I-CCD camera (Andor, iStar 340). By switching between a mirror and a grating (150 l/mm groove density; blaze = 500 NM), the spectrometer can be used for imaging and spectroscopy respectively. The latter option requires closing the slit of the spectrometer to ensure adequate spectral resolution. For the bright field imaging, an LED source mounted above the sample was used. This LED source could be polarization selected by a broadband polarizing sheet, positioned perpendicular to a rotatable broadband polarizer in the detection path. In this manner, polarized optical microscopy images could be recorded.

Synthetic details for compounds ***(S)*-BPM-4-C4(1)**, ***(S)*-BPM-3,4-C4(1) and *(S)*-BPM-3,5-C4(1)**: **Compound *(S)*-BPM-4-C4(1)**: *(S)*-4-(2-methylbutoxy) benzaldehyde (2.3 mmol, 0.45 g) and 4,4′,6,6′-tetramethyl-2,2′-bipyrimidine (0.46 mmol, 0.1 g) were added in an aqueous solution of NaOH (5 M) (15 ml). Aliquat 336 (10% mol, 21 μL, 3 drops) was added. The solution was refluxed for 48 h. After cooling the solution, the precipitate was filtrated and washed with water. The crude was solubilized in DCM, washed with water, dried over $MgSO_4$ and concentrated under reduced pressure. The crude product was purified by silica gel chromatography (100% PE gradually to 100% DCM in 30 min). The product ***(S)*-BPM-4-C4(1)** was precipitated by slow evaporation of a DCM/MeOH mixture. Compound ***(S)*-BPM-4-C4(1)** was obtained as a yellow powder (0.083 g, 20%). ^{1}H NMR (300 MHz, $CDCl_3$) δ 7.95 (d, *J* = 16.1 Hz, 4H, $CH_{ethylenic}$), 7.60 (d, *J* = 8.9 Hz, 8H, $CH_{aromatic}$), 7.52 (s, 2H, CH_{BPM}), 7.18 (d, *J* = 16.1 Hz, 4H, $CH_{ethylenic}$), 6.94 (d, *J* = 8.8 Hz, 8H, $CH_{aromatic}$), 3.90–3.76 (m, 8H, OCH_2), 1.97–1.81 (m, 4H, C*H), 1.66–1.52 (m, 4H, C*CH_2), 1.36–1.21 (m, 4H, C*CH_2), 1.03 (d, *J* = 6.7 Hz, 12H, C*CH_3), 0.96 (t, *J* = 7.5 Hz, 12H, CH_3).^{13}C NMR (75 MHz, $CDCl_3$) δ 164.29 (C_{quat}), 163.69 (C_{quat}), 160.58 (C_{quat}), 137.07 ($CH_{ethylenic}$), 129.29 ($CH_{aromatic}$), 128.62 (C_{quat}), 124.45 ($CH_{ethylenic}$), 115.04 ($CH_{aromatic}$), 113.95 ($CH_{aromatic}$), 73.12 (OCH_2), 34.82 (C*H), 26.27 (CH_2), 16.67 (C*$\underline{C}H_3$), 11.45 (CH_3). *m/z* (Maldi-TOF) 910.38 ([M]$^+$, $C_{60}H_{70}N_4O_4$ requires 910.54). Elem. Anal.: C, 79.34; H, 7.95; N, 6.24; $C_{60}H_{70}N_4O_4$ requires C, 79.09; H, 7.74; N, 6.15.

Compound ***(S)*-BPM-3,4-C4(1)**: 3,4-bis((*S*)-2-methylbutoxy) benzaldehyde (0.83 mmol, 0.232 g) and 4,4′,6,6′-tetramethyl-2,2′-bipyrimidine (0.17 mmol, 0.036 g) were added in an aqueous solution of NaOH (5 M) (15 ml). Aliquat 336 (10% mol, 8 μL, 1 drop) was added. The solution was refluxed for 48 h. After cooling the solution, the precipitate was filtrated and washed with water. The crude was solubilized in DCM, washed with water, dried over $MgSO_4$ and concentrated under reduced pressure. The crude product was purified by silica gel chromatography (100% PE gradually to 100% DCM in 30 min). The product ***(S)*-BPM-3,4-C4(1)** was precipitated by slow evaporation of a DCM/MeOH mixture. Compound ***(S)*-BPM-3,4-C4(1)** was obtained as yellow powder (0.130 g, 61%). ^{1}H NMR (300 MHz, $CDCl_3$) δ 7.85 (d, J = 16.1 Hz, 4H, $CH_{ethylenic}$), 7.61 (s, 2H, CH_{BPM}), 7.25–7.11 (m, 12H, 4 $CH_{ethylenic}$, 8 $CH_{aromatic}$), 6.89 (d, J = 8.3 Hz, 4H, $CH_{aromatic}$), 3.94–3.79 (m, 16H, OCH_2), 2.00–1.87 (m, 8H, C*H), 1.70–1.54 (m, 8H, CH_2), 1.39–1.23 (m, 8H, CH_2), 1.08 (d, J = 6.8 Hz, 12H, C*CH_3), 1.07 (d, J = 6.8 Hz, 12H, C*CH_3), 0.98 (t, J = 7.5 Hz, 12H, CH_3), 0.96 (t, J = 7.5 Hz, 12H, CH_3). ^{13}C NMR (75 MHz, $CDCl_3$) δ 164.12 (C_{quat}), 163.77 (C_{quat}), 150.90 (C_{quat}), 149.60 (C_{quat}), 137.13 ($CH_{aromatic}$), 128.85 (C_{quat}), 124.71 ($CH_{ethylenic}$), 122.00 ($CH_{ethylenic}$), 113.20 ($CH_{aromatic}$), 112.88 ($CH_{aromatic}$), 111.65 ($CH_{aromatic}$), 74.08 (OCH_2), 73.88 (OCH_2), 34.86 (C*H), 34.80 (C*H), 26.22 (CH_2), 26.18 (CH_2), 16.59 (C*$\underline{C}H_3$), 16.55 (C*$\underline{C}H_3$), 11.38 (CH_3), 11.36 (CH_3). *m/z* (Maldi-TOF) 1255.4 ($[M]^+$, $C_{80}H_{110}N_4O_8$ requires 1255.53). Elem. Anal.: C, 72.53; H, 8.46; N, 4.23; $C_{80}H_{11}N_4O_8.CH_2Cl_2$ requires C, 72.57; H, 8.42; N, 4.18.

Compound ***(S)*-BPM-3,5-C4(1)**: 3,5-bis((*S*)-2-methylbutoxy) benzaldehyde (1.1 mmol, 0.3 g) and 4,4′,6,6′-tetramethyl-2,2′-bipyrimidine (0.22 mmol, 0.047 g) were added in an aqueous solution of NaOH (5 M) (15 ml). Aliquat 336 (10% mol, 10 μL, 2 drops) was added. The solution was refluxed for 48 h. After cooling the solution, the precipitate was filtrated and washed with water. The crude was solubilized in DCM, washed with water, dried over $MgSO_4$ and concentrated under reduced pressure. The crude product was purified by silica gel chromatography (100% PE gradually to 100% DCM in 30 min). The product **(S)-BPM-3,5-C4(1)** was precipitated by slow evaporation of a DCM/MeOH mixture. Compound ***(S)*-BPM-3,5-C4(1)** was obtained as yellow powder (0.129 g, 47%).^{1}H NMR (300 MHz, $CDCl_3$) δ 7.84 (d, J = 16.2 Hz, 4H, $CH_{ethylenic}$), 7.67 (s, 2H, CH_{BPM}), 7.33 (d, J = 16.2 Hz, 4H, $CH_{ethylenic}$), 6.81 (d, J = 2.2 Hz, 8H, $CH_{aromatic}$), 6.50 (t, J = 2.2 Hz, 4H, $CH_{aromatic}$), 3.88–3.74 (m, 16H, OCH_2), 1.94–1.83 (m, 8H, C*H), 1.66–1.52 (m, 8H, CH_2), 1.35–1.21 (m, 8H, CH_2), 1.03 (d, J = 6.7 Hz, 24H, C*CH_3), 0.97 (t, J = 7.4 Hz, 24H, CH_3). ^{13}C NMR (75 MHz, $CDCl_3$) δ 164.08 (C_{quat}), 163.94 (C_{quat}), 160.83 (C_{quat}), 137.64 ($CH_{aromatic}$), 127.25 ($CH_{ethylenic}$), 113.70 ($CH_{aromatic}$), 106.06 ($CH_{aromatic}$), 103.10 ($CH_{ethylenic}$), 73.17 (OCH_2), 34.80 (C*H), 26.25 (CH_2), 16.66 (C*$\underline{C}H_3$), 11.44 (CH_3). *m/z* (Maldi-TOF) 1255.56 ($[M-H]^-$, $C_{80}H_{110}N_4O_8$ requires 1254.83). Elem. Anal. : C, 76.35; H, 9.05; N, 4.35; $C_{80}H_{11}N_4O_8$ requires C, 76.52; H, 8.83; N, 4.46.

Acknowledgements

This research has been supported by the French National Research Agency (ANR), in the framework of the 3D-ODS research program (Project-ANR-20-CE24-0028) and by the "région Bretagne" in the framework of the 3D-STORE research program (Project N° 241302 – UMR6226).

Conflict of Interests

The authors declare no conflict of interest.

Data Availability Statement

The data that support the findings of this study are available from the corresponding author upon reasonable request.

Keywords: Bipyrimidine · Chirality · Molecular organisation · Nonlinear Optic · Thin Films

[1] a) A. Aghigh, S. Bancelin, M. Rivard, M. Pinsard, H. Ibrahim, F. Légaré, *Biophys. Rev. Lett.* **2023**, *15*, 43–70; b) J. Frigerio, C. Ciano, J. Kuttruff, A. Mancini, A. Ballabio, D. Chrastina, V. Falcone, M. De Seta, L. Baldassarre, J. Allerbeck, D. Brida, L. Zeng, E. Olsson, M. Virgilio, M. Ortolani, *ACS Photonics* **2021**, *8*, 3573–3582; c) G. Q. Ngo, E. Najafidehaghani, Z. Gan, S. Khazaee, M. Per Siems, A. George, E. P. Schartner, S. Nolte, H. Ebendorff-Heidepriem, T. Pertsch, A. Tuniz, M. A. Schmidt, U. Peschel, A. Turchanin, F. Eilenberger, *Nat. Photonics* **2022**, *16*, 769–776; d) R.-C. Xiao, D.-F. Shao, W. Gan, H.-W. Wang, H. Han, Z. G. Sheng, C. Zhang, H. Jiang, H. Li *npj Quantum Materials* **2023**, *8*, 62; e) V. V. Nautiyal, P. Silotia, *Phys. Lett. A* **2018**, *382*, 2061–2068; f) L. Schneider, W. Peukert, *Part. Part. Syst. Charact.* **2006**, *23*, 351–359; g) W. R. Zipfel, R. M. Williams, W. W. Webb, *Nat. Biotechnol.* **2003**, *21*, 1369; h) F. Helmchen, W. Denk, *Nat. Methods* **2005**, *2*, 932; i) V. Van Steenbergen, W. Boesmans, Z. Li, Y. de Coene, K. Vints, P. Baatsen, I. Dewachter, M. Ameloot, K. Clays, P. Vanden Berghe, *Nat. Commun.* **2019**, *10*, 3530; j) H. Xu, D. L. Elder, L. E. Johnson, Y. de Coene, S. R. Hammond, W. Vander Ghinst, K. Clays, L. R. Dalton, B. H. Robinson, *Adv. Mater.* **2021**, *33*, 2104174; k) Y. Shi, C. Zhang, H. Zhang, J. H. Bechtel, L. R. Dalton, B. H. Robinson, W. H. Steier, *Science* **2000**, *288*, 119.

[2] a) I. Ionita, A. Bercea, S. Brajnicov, A. Matei, V. Ion, V. Marascu, B. Mitu, C. Constantinescu, *Appl. Surf. Sci.* **2019**, *480*, 212–218; b) C. Wang, X. Xiong, N. Andrade, V. Venkataraman, X.-F. Ren, G.-C. Guo, M. Lončar, *Opt. Express* **2017**, *25*, 6963–6973.

[3] a) Z. Sekkat, W. Knoll, *Photoreactive Organic Thin Films*, John Wiley & Sons, Ltd, **2002**; b) D. S. Chemla, J. Zyss, *Nonlinear Optical Properties of Organic Molecules and Crystals*, Academic Orlando, FL, **1987**; c) I. Ionita, A. Bercea, S. Brajnicov, A. Matei, V. Ion, V. Marascu, B. Mitu, C. Constantinescu, *Appl. Surf. Sci.* **2019**, *480*, 212–218; d) H. Nalwa, S. Miyata, *Nonlinear Optics of Organic Molecules and Polymers*, CRC Press, Boca Raton, FL, **1996**, p 397.

[4] Nummerierung?a) K. Iliopoulos, O. Krupka, D. Gindre, M. Sallé, *J. Am. Chem. Soc.* **2010**, *132*, 14343–14345; b) D. Gindre, K. Iliopoulos, O. Krupka, M. Evrard, *Molecules* **2016**, *21*, 147; c) E. Champigny, M. Sallé, M. C. Spiridon, K. Iliopoulos, F. A. Jerca, V. V. Jerca, D. M. Vuluga, D. S. Vasilescu, D. Gindre, B. Sahraoui, *Dyes Pigm.* **2015**, *114*, 24–32; d) D. Gindre, A. Boeglin, A. Fort, L. Mager, K. D. Dorkenoo, *Opt. Express* **2006**, *14*, 9896.

[5] a) D. Gindre, E. Champigny, K. Iliopoulos, O. Krupka, Y. Morille, M. Sallé, *Opt. Lett.* **2013**, *38*, 4636–4639; b) D. Gindre, K. Iliopoulos, O. Krupka, E. Champigny, Y. Morille, M. Sallé, *Opt. Lett.* **2013**, *38*, 4636; c) Z. J. Hou, L. Y. Liu, J. Chen, L. Xu, Z. L. Xu, W. C. Wang, F. M. Li, M. X. Ye, *Phys. Lett. A* **1999**, *252*, 87–91.

[6] a) T. L. Penner, H. R. Motschmann, N. J. Armstrong, M. C. Ezenyilimba, D. J. Williams, *Nature* **1994**, *367*, 49–51; b) H. Schwartz, R. Mazor, V. Khodorkovsky, L. Shapiro, J. T. Klug, E. Kovalev, G. Meshulam, G. Berkovic, Z. Kotler, S. Efrima, *J. Phys. Chem. B* **2001**, *105*, 5914–5921; c) S. Schrader, V. Zauls, B. Dietzel, C. Flueraru, D. Prescher, J. Reiche, H. Motschmann, L. Brehmer, *Mater. Sci. Eng. C* **1999**, *8–9*, 527–537.

[7] S. van Cleuvenbergen, P. Kędziora, J. L. Fillaut, T. Verbiest, K. Clays, H. Akdas-Kilig, F. Camerel, *Angew. Chem. Int. Ed.* **2017**, *56*, 9546–9550.

[8] U. Bora, S. Abdallah, R. Mhanna, P. Nicolas, A. Dok, Y. de Coene, S. Van Cleuvenbergen, O. Jeannin, J. P. Malval, K. Clays, N. Bellec, H. Ocak, B. Bilgin-Eran, F. Camerel, H. Akdas-Kiliç, *Chem. A Eur. J.* **2024**, *30*, 1–11.

[9] J. Nasielski, A. Standaert, R. Nasielski-Hinkens, *Synth. Commun.* **1991**, *21*, 901–906.

[10] X. Ma, E. A. Azeem, X. Liu, Y. Cheng, C. Zhu, *J. Mater. Chem. C* **2014**, *2*, 1076–1084.

[11] F. Bellotta, M. V. D'Auria, V. Sepe, A. Zampella, *Tetrahedron* **2009**, *65*, 3659–3663.

[12] H. Akdas-Kilig, M. Godfroy, J. L. Fillaut, B. Donnio, B. Heinrich, P. Kędziora, J. P. Malval, A. Spangenberg, S. Van Cleuvenbergen, K. Clays, F. Camerel, *J. Phys. Chem. C* **2015**, *119*, 3697–3710.

[13] C. Lambert, G. Nöll, E. Schmälzlin, K. Meerholz, C. Bräuchle, *Chem. Eur. J.* **1998**, *4*, 512–521.
[14] F. Terenziani, C. Katan, E. Badaeva, S. Tretiak, M. Blanchara-Desce, *Adv. Mater.* **2008**, *20*, 4641–4678.
[15] D. Beljonne, W. Wenseleers, E. Zojer, Z. Shuai, H. Vogel, S. J. K. Pond, J. W. Perry, S. R. Marder, J. L. Brédas, *Adv. Funct. Mater.* **2002**, *12*, 631–641.
[16] J. R. . Frisch, M. J.; Trucks, G. W.; Schlegel, H. B.; G. E. Scuseria; Robb, M. A.; Cheesemam, J. . J. A. Montgomery, J.; Vreven, T.; Kudin, K. N.; Burant, J. C.; Millam, J. M.; Lyengar, S. S.; Tomasi, H. . H. Barone, V.; Mennucci, B.; Cossi, M.; Scalmani, G.; Rega, N.; Petersson, G. A.; Nakatsuji, O. . M.; Ehara, M.; K. Toyota; Fukuda, R.; Hasegawa, J.; Ishida, M.; Nakajima, T.; Honda, Y.; Kitao, J. . Nakai, H.; Klene, M.; Li, X.; Knox, J. E.; Hratchian, H. P.; Cross, J. B.; Adamo, C.; Jaramillo, J. W. . Gomperts, R.; Stratmann, R. E.; Yazyev, O.; Austin, A. J.; Cammi, R.; Pomelli, C.; Ochterski, V. G. . Ayala, P. Y.; Morokuma, K.; Voth, G. A.; Salvador, P.; Dannenberg, J. J.; Zakrzewski, A. D. . R. Dapprich, S.; Daniels, A. D.; Strain, M. C.; Farkas, O.; Malick, D. K.; Rabuck, B. B. . K.; Foresman, J. B.; Ortiz, J. V.; Cui, Q.; Baboul, A. G.; Clifford, S.; Cioslowski, J.; Stefanov, M. Liu, G.; Liashenko, A.; Piskorz, P.; Komaromi, I.; Martin, R. L.; Fox, D. J.; Keith, T.; Al-Laham, M. A.; Peng, C. Y.; Nanayakkara, A.; Challacombe, M.; Gill, P. M. W.; Johnson, B.; Chen, W.; Wong, J. A. W.; Gonzalez, C.; Pople, *Gaussian 03, Revis. B.03, Pittsburgh PA* **2003**.
[17] J. M. Roy Dennington, Todd Keith, *GaussView, Version 6.1.1, Semichem Inc., Shawnee Mission. KS* **2019**.
[18] B. Barszcz, A. Bogucki, R. Świetlik, H. Akdas-Kiliç, F. Camerel, T. Roisnel, *Liq. Cryst.* **2019**, *46*, 1403–1414.
[19] T. Ishikawa, A. Honda, K. Miyamura, *CrystEngComm* **2022**, *24*, 5900–5906.
[20] C. Xu, W. Denk, W. W. Webb, J. Guild, *Opt. Lett.* **1995**, *20*, 2372–2374.
[21] M. A. Albota, C. Xu, W. W. Webb, *Appl. Opt.* **1998**, *37*, 7352.
[22] N. S. Makarov, M. Drobizhev, A. Rebane, B. H. Cumpston, S. P. Anantha-vel, S. Barlow, D. L. Dyer, J. E. Ehrlich, L. L. Erskine, A. A. Heikal, S. M. Kuebler, I.-Y. S. Lee, D. Mccord-Maughon, J. Qin, H. Rockel, M. Rumi, X.-L. Wu, S. R. Marder, J. W. Perry, A. Karotki, M. Kruk, M. Drobizhev, A. Rebane, E. Nickel, C. W. Spangler, *Opt. Express* **2008**, *16*, 4029–4047.
[23] S. de Reguardati, J. Pahapill, M. Rammo, A. Rebane, *Opt. Express* **2016**, *24*, 9053–9066.
[24] S. R. Meech, D. Phillips, *J. Photochem.* **1983**, *23*, 193–217.
[25] D. P. D. V. Connor, *Time-Correlated Single Photon Counting*, Elsevier, **1984**.

Manuscript received: January 31, 2024
Revised manuscript received: February 13, 2024
Accepted manuscript online: February 14, 2024
Version of record online: February 29, 2024